Measurement of the mercury (6s6p) 3P1-state lifetime in the frequency domain from integrated absorbance data

Measurement of the mercury $(6s6p)\ ^3P_1$-state lifetime in the frequency domain from integrated absorbance data

S. Gravina,[1] C. Clivati,[2] A. Castrillo,[1] E. Fasci,[1] N. A. Chishti,[1] G. Galzerano,[3] F. Levi,[2] and L. Gianfrani[1,*]

[1]*Dipartimento di Matematica e Fisica, Università degli Studi della Campania "Luigi Vanvitelli", 81100 Caserta, Italy*

[2]*Istituto Nazionale di Ricerca Metrologica (INRiM), 10135 Torino, Italy*

[3]*Istituto di Fotonica e Nanotecnologie, Consiglio Nazionale delle Ricerche, 20133 Milano, Italy*

(Received 1 July 2022; accepted 12 August 2022; published 26 September 2022)

Quantitative UV laser absorption spectroscopy is implemented to measure the strength of the $(6s^2)\ ^1S_0 \rightarrow (6s6p)\ ^3P_1$ intercombination transition of Hg atoms near the wavelength of 253.7 nm and to retrieve the lifetime of the excited state. Tunable, single-mode, coherent radiation in the deep UV is produced through a double-stage second-harmonic generation process, starting from the output radiation of an external-cavity diode laser at 1014.8 nm. This latter is referenced to an optical frequency comb synthesizer. The measurement strategy exploits the relationship between the strength of an optical transition and the spontaneous emission Einstein coefficient. The complete uncertainty budget leads to an overall relative uncertainty of 0.6%, with a statistical contribution of 0.28 ns, which is the lowest ever obtained for the $(6s6p)\ ^3P_1$ lifetime. The new value, amounting to 125.12 ± 0.79 ns, compares well with most of the past determinations within two times the quoted uncertainties. Despite this, it does not agree with the weighted average of the 12 prior values, thus suggesting that a critical reassessment of the uncertainty of some of the past measurements is probably necessary.

DOI: 10.1103/PhysRevResearch.4.033240

I. INTRODUCTION

The $(6s^2)\ ^1S_0 \rightarrow (6s6p)\ ^3P_1$ intercombination transition of mercury at 253.7 nm is of particular interest for a variety of fundamental studies and applications. Normally used for laser cooling and trapping of mercury vapors [1], the transition plays a crucial role in the search for a permanent electric dipole moment of the ^{199}Hg atom [2], as well as in the development of an optical lattice clock in the deep UV [3]. It is also a highly sensitive probe of possible long-term variations of the fine-structure constant [4]. Selective reflection of light at the interface between a dielectric medium and a resonant vapor was observed, for the first time, by looking at the mercury intercombination line [5]. Such a technique is, nowadays, a powerful tool to study the Casimir–Polder interaction [6]. Space observations of the Hg deep-UV spectrum provide precious information about the overabundances and isotope anomalies of mercury in HgMn stars, a subgroup of hot, chemically peculiar stars [7–9].

Recently, the spectral line at 253.7 nm has been used for the spectroscopic determination of absolute concentrations of atmospheric mercury [10,11]. To this aim, a weighted average of 12 prior determinations of the $(6s6p)\ ^3P_1$ state lifetime was adopted as the best way to specify the spontaneous emission Einstein coefficient, from which the line strength factor could be retrieved [10,12]. Nevertheless, among the 12 contributing values of Curtis *et al.* [12], the one with the largest statistical weight—namely, 120.0 ± 0.7 ns, resulting from an electron–photon delayed coincidence apparatus [13]—is roughly 50 years old, while the most recent determination, as obtained by means of time-resolved laser-induced fluorescence spectroscopy [14], 125 ± 6 ns, exhibits a much larger uncertainty. It should be noted that the uncertainty of 0.7 ns reported by King and Adams [13] is of statistical origin and does not include systematic effects, as clearly stated by the authors in their concluding sentence. In fact, systematic errors were judged to be negligible. On the other hand, the functional form of the spectrum was assumed to be the convolution of a Gaussian instrumental profile with an exponential decay, and the impact of such a profile on the accuracy of the lifetime measurement was not discussed. This situation points to the need for new, accurate, and reliable measurements to verify whether the weighted mean, equal to 118.9 ± 0.4 ns, as reported by Curtis *et al.* [12], could be affected by a significant bias.

We report on the development and application of a high-resolution absorption spectrometer that allowed us to measure the $(6s6p)\ ^3P_1$ state lifetime with a subpercent accuracy. The measurement procedure exploits the fact that the spontaneous emission Einstein coefficient of the intercombination line, $A_{2,1}$, is equal to the reciprocal of the $(6s6p)\ ^3P_1$ state lifetime (τ_2), since the transition is closed. Linear absorption spectroscopy is performed, with a frequency scale calibrated by means of a near-infrared optical frequency comb synthesizer.

*livio.gianfrani@unicampania.it

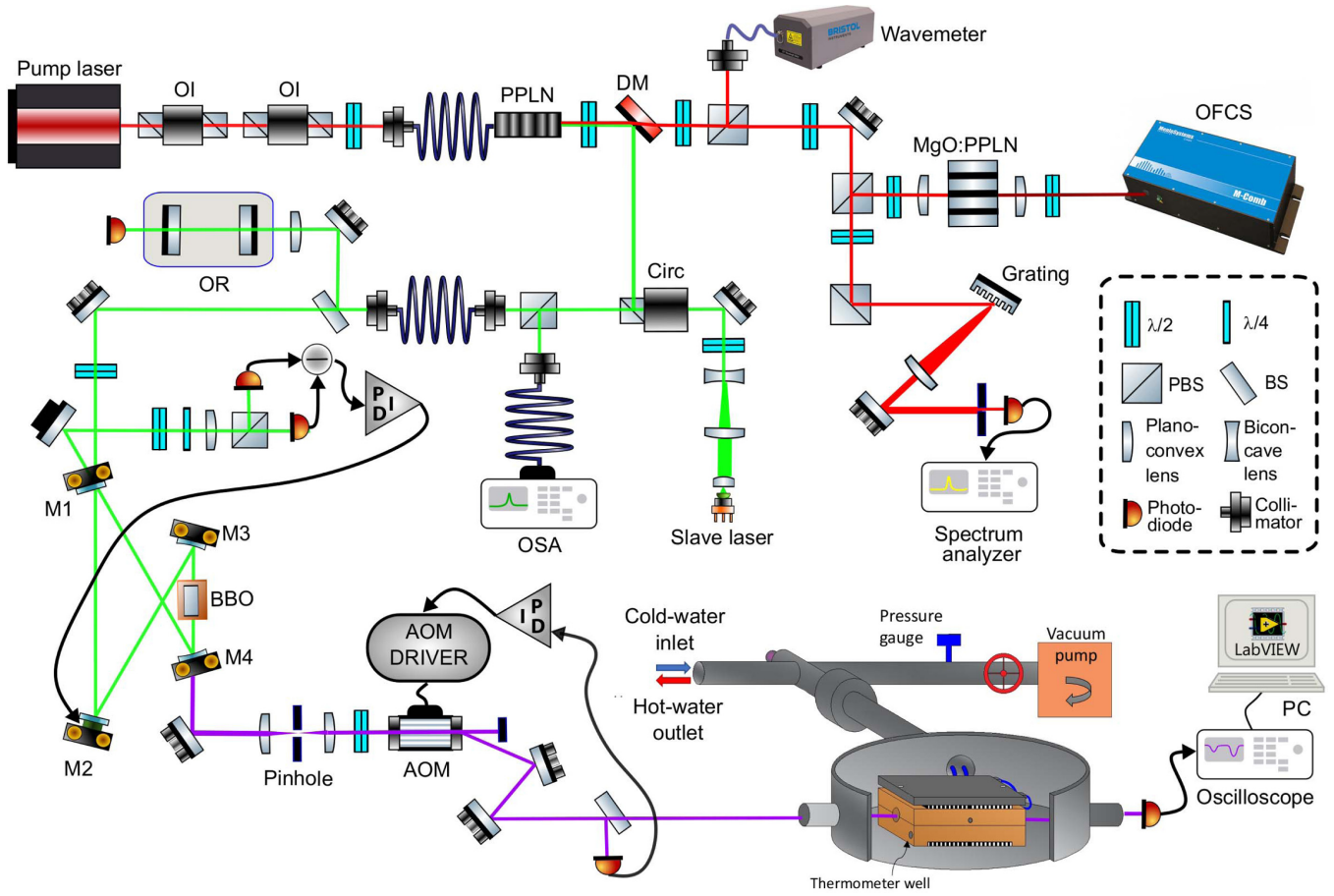

FIG. 1. Schematic diagram of the UV absorption spectrometer. OI, optical isolator; PPLN, periodically poled lithium niobate crystal waveguide; DM, dichroic mirror; PBS, polarizing beam splitter; BS, beam splitter; MgO: PPLN, magnesium-doped lithium niobate crystal; $\lambda/2$, half-wave plate; OFCS, optical frequency comb synthesizer; Circ, circulator; OR, optical resonator; $\lambda/4$, quarter-wave plate; PID, proportional–integral–derivative circuit; M, mirror; BBO, beta-barium borate crystal; OSA, optical spectrum analyzer; AOM, acousto-optic modulator; PC, personal computer.

II. METHOD

The absorption process occurring when the UV laser beam propagates into the mercury gas cell, at a frequency ν resonant with the intercombination line, is ruled by the well-known Lambert-Beer law, which states that the transmitted power P decreases as follows:

$$P(\nu) = P_0 \exp\left[-S_{1,2} g(\nu - \nu_0) LN\right], \tag{1}$$

where P_0 is the incident power, ν_0 is the line-center frequency, L is the absorption path length, N is the atomic number density of the absorbing isotopic species, $S_{1,2}$ is the transition strength, and $g(\nu - \nu_0)$ is the normalized line shape function. The transition strength is related to $A_{2,1}$ through the expression [10]

$$S_{1,2} = \frac{1}{8\pi} \frac{g_2}{g_1} \frac{c^2}{\nu_{1,2}^2} A_{2,1}, \tag{2}$$

where c is the vacuum speed of light, and g_1 and g_2 are the quantum degeneracies of the ground and excited states, respectively, as determined from the total angular momentum quantum numbers.

A simple expression for the integrated absorbance, A_T, can be derived from Eq. (1):

$$A_T = \int \ln\left[\frac{P_0}{P(\nu)}\right] d\nu = S_{1,2} LN. \tag{3}$$

Tuning the laser frequency continuously around the line center, one can accurately measure the transmitted intensity as a function of the frequency. Repeating the measurements at different Hg vapor pressures, it is possible to retrieve the transition strength from a linear fit of the frequency-integrated absorbance versus N, provided that L is known. Therefore, the upper state lifetime can be determined by inverting Eq. (2), thus leading to the following equation:

$$\tau_2 = \frac{1}{8\pi} \frac{g_2}{g_1} \frac{c^2}{\nu_{1,2}^2} \frac{1}{S_{1,2}}. \tag{4}$$

III. EXPERIMENTAL SETUP

The experimental setup, which is depicted in Fig. 1, essentially consists of an UV laser source, a temperature-stabilized mercury vapor cell, a silicon–carbide (SiC) photodetector, and

a data acquisition chain. The UV laser source is described in detail in Ref. [15].

It is based on a two-stage second-harmonic generation (SHG) scheme in a pair of nonlinear crystals. An external cavity diode laser (ECDL) operating at 1014.8 nm is used as a pump laser, providing an optical power of about 80 mW. Using a single passage through a fiber-coupled periodically poled lithium niobate crystal waveguide, the radiation emitted by the ECDL is converted from the near-infrared (NIR) region to the visible at 507.4 nm. A dichroic mirror separates the second-harmonic radiation and the residual NIR component. This latter is divided into two parts: The first portion is sent to a nine-digit wavemeter to measure the emission wavelength constantly; the other part is employed for comb referencing by means of a new scheme that is illustrated later. The produced radiation at 507.4 nm seeds a high-power diode laser (Nichia NDE4116), hereafter referred to as a slave laser, at the same wavelength, thus amplifying the optical power up to five times by injection locking. Once the mode matching of the slave and seed beams is optimized, stable and single-mode operation can be maintained for several hours. A portion of the green radiation is coupled to a 50-cm-long optical resonator that is used for frequency calibration purposes. It consists of a pair of identical, high-quality, 1-inch dielectric mirrors with a radius of curvature of 100 cm and a reflectivity of about 99% at 507 nm. The mirror mounts, tightly locked over a stainless steel base, fit into the two ends of a glass tube, which is periodically evacuated. The resonator is housed inside a thermal insulating box.

The second stage of second-harmonic generation from 507.4 nm to 253.7 nm is obtained through a 12-mm long beta-barium borate (BBO) crystal placed inside a bow-tie resonant cavity, locked to the incident beam by means of the Hänsch–Couillaud technique [16]. The output UV power amounts to about 250 μW when the green input power is 15 mW. To improve the spatial quality of the UV beam, which is limited by the BBO crystal walk-off, the radiation is focused into a 50-μm pinhole and then collimated. The UV radiation passes through an acousto-optic modulator (AOM), which is used to stabilize the UV power in a new configuration, as compared to the one adopted previously [15]. A part of the first-order diffracted UV light is monitored by a SiC photodetector to actively control the RF power driving the AOM, thus stabilizing the UV light power. The relative power stability (as measured at a constant laser frequency) resulted to be better than 10^{-4} over the typical duration of the spectroscopy sessions, i.e., about 20 minutes.

The remaining portion of the produced UV laser beam, with a power of about 0.2 μW and a diameter of 4 mm, is sent to a 2-mm-long cylindrical quartz cell (with a 2-cm diameter), sealed at the two ends by a pair of Spectrosil® far-UV quartz windows and equipped with a small reservoir in the middle of its length (as provided by Precision Glassblowing Inc.). The reason for such a short cell comes from the relatively large vapor pressures of mercury that cause strong attenuation of the laser beam. For instance, using a 2-cm-long cell, at room temperature, the line-center fractional absorption for the most abundant isotope would be close to 100%, in coincidence with the intercombination transition. As guaranteed by the manufacturer, the reservoir is filled with liquid mercury and the cell is closed under a 10^{-10}-Pa vacuum environment, so as to have ultrapure Hg vapors in equilibrium with the liquid phase. The cell is placed in a homemade hollow copper block, equipped with a well where the cell's reservoir perfectly fits. The block is housed inside a stainless steel vacuum chamber, sealed with a pair of antireflection (AR)-coated 1-inch quartz windows. The block temperature is actively stabilized by using a few Peltier elements, driven by a proportional–integral–derivative controller. Temperature reading, which is one of the key points of this work, is provided by a precision platinum resistance thermometer (Pt100) that is properly housed in the copper block and connected to a 6½-digit multimeter. The entire system, calibrated at the National Metrology Institute, provides a temperature stability and accuracy for the mercury cell of about 0.01 K, in the temperature interval between 250 K and 320 K, as tested by doing continuous measurements over several days. Temperature gradients over the copper block length are quoted to be negligible. After the interaction with Hg vapors, the transmitted UV radiation is focused on a SiC photodetector.

The NIR ECDL and, consequently, the UV source can operate in two different configurations: free-running and comb-locked modes. In the first case, continuous frequency scans of the UV radiation are possible by tuning the NIR ECDL frequency at a rate of about 1 Hz and using a feed-forward scheme for the injection current of the slave laser. In so doing, injection from the seed light can be maintained throughout the full frequency scan, while the bow-tie cavity remains tightly locked to the green radiation. In this configuration, the UV radiation continuously covers a frequency interval as wide as 15 GHz.

In the second configuration, the ECDL NIR radiation is referenced to an optical frequency comb synthesizer (FC1500-250-WG, MENLO Systems) based on an erbium-doped, mode-locked femtosecond fiber laser at 1560 nm. Both the comb repetition rate (f_{rep}) and the carrier-envelope offset frequency were stabilized against a GPS-disciplined rubidium clock, thus providing a self-referenced supercontinuum spanning one octave at wavelengths from 1050 nm to 2100 nm. Since the ECDL wavelength is out of this range, some additional efforts were necessary to implement the comb-locked mode. More particularly, we performed a SHG process of the longer wavelength portion of the comb (above 2 μm) in a 3-mm-long MgO-doped periodically poled lithium niobate crystal to produce comb radiation centered at 1020 nm with a width of about 20 nm and a peak power of 1 μW, as measured by means of an optical spectrum analyzer at the resolution bandwidth of 1 nm. Input and output facets of the crystal have an AR coating from 1968 nm to 2270 nm and from 984 nm to 1135 nm, respectively. The SHG crystal output is overlapped with the ECDL NIR beam, spectrally filtered by a grating–lens–slit assembly, and sent to a fast photodiode. The beat note between the NIR laser and the nearest tooth of the minicomb could be detected with a 30-dB signal-to-noise ratio at a resolution bandwidth of 1 kHz. Such a signal was effectively used to lock the NIR ECDL to the comb with an offset frequency of 20 MHz. A tight lock condition was achieved by comparing the beat note with a local oscillator and by feeding the error signal back to the diode laser current after proper amplification and integration. Highly accurate

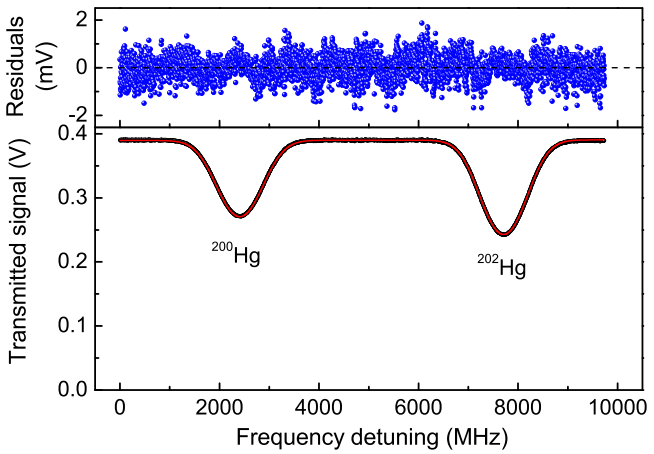

FIG. 2. Experimental transmission spectrum across the intercombination transition of the ^{200}Hg and ^{202}Hg isotopes at a vapor pressure of about 56 mPa and a temperature of 280.65 (1) K. Fit residuals, reported in the upper plot, exhibit a root-mean-square value of 480 μV. The resulting signal-to-noise ratio amounts to ∼800. The same level of agreement between theory and experiment was obtained in the entire pressure range.

and reproducible frequency scans of the ECDL frequency were performed by finely tuning the comb repetition rate. More particularly, a scan of $f_{\rm rep}$ of 750 Hz yielded a NIR frequency tuning of about 900 MHz, which translates into a 3.6-GHz wide scan in the UV domain. This is about a factor of 4 narrower than that achievable in the free-running mode. Unfortunately, the locking electronics acting on the ECDL do not support larger scans in the current configuration.

The comb-locked way of operation was used to measure the free spectral range (FSR) frequency of the optical resonator at 507.4 nm. To this aim, repeated acquisitions of the cavity output spectra were performed while doing comb-calibrated frequency scans. The weighted mean of the retrieved FSR values gives a result of 300.07 ± 0.35 MHz, which is in agreement with the one retrieved from the length of the optical resonator.

In the free-running configuration, the signal transmitted from the mercury cell, the one transmitted from the optical resonator, and the Pt100 resistance were simultaneously acquired. Each absorption spectrum consists of 5000 points that were registered with a 16-bit vertical resolution. Spectral averaging over five consecutive scans was also performed.

IV. RESULTS

The example spectrum of Fig. 2 shows the line profiles in coincidence with the ^{200}Hg and ^{202}Hg bosonic isotopes over a frequency interval of about 10 GHz, as obtained by using the free-running mode of operation. A MATLAB code was developed to perform the frequency calibration, to carry out line fits and retrieve the integrated absorbance in a fully automated way for any set of repeated acquisitions. Particular attention was paid to the frequency scale underneath each spectrum. In fact, prior to each fit, the code analyzed the transmission spectrum from the optical resonator in order to construct a linear frequency scale underneath the corresponding absorption spectrum. Such a scale was obtained as a result of a cubic spline interpolation of the peak frequencies versus their index in the data array. Using the Levenberg-Marquardt aldorithm, each mercury spectrum was compared to the following function:

$$P(\nu) = (w_0 + w_1\nu)e^{-\{A_{T1}[g(\nu-\nu_{01})]+A_{T2}[g(\nu-\nu_{02})]\}}, \qquad (5)$$

where, compared to Eq. (1), a linear frequency dependence in the baseline is included to account for residual power variations due to the ECDL frequency tuning, ν is the UV frequency, ν_{0x} is the line-center frequency (the subscript $x = 1$ and 2 standing for ^{200}Hg and ^{202}Hg, respectively), and A_{Tx} is the integrated absorbance. The experimental profiles are well described by a Voigt convolution, as shown by the absolute residuals reported in the upper plot of Fig. 2, computed as deviations between theory and experiment. The Doppler full width at half-maximum (FWHM) of each line is set to the value that is determined by the thermodynamic temperature T of the vapor cell. The homogeneous linewidth is shared among the two isotopes and treated as a free parameter. As a result, the fitting code managed, in each run, 5000 points and seven free parameters associated with the Hg spectra. The residuals of Fig. 2 do not show any evidence of line profile distortion that could be ascribed to a residual nonlinearity of the frequency scale.

Repeated acquisitions of mercury spectra were performed as a function of the cell's temperature, in the range between 278.65 K and 293.15 K, which corresponds to Hg vapor pressures from 46 mPa to 168 mPa. The vapor pressures were determined with a relative uncertainty of 1% by using the Wagner-type equation reported by Huber *et al.* [17]. The vapor pressure is given by the following equation [17]:

$$\ln(p/p_c) = (T_c/T)(a_1\tau + a_2\tau^{1.89} + a_3\tau^2 + a_4\tau^8 + a_5\tau^{8.5} + a_6\tau^9), \qquad (6)$$

where p_c and T_c are the critical point pressure and temperature of mercury, respectively; τ is equal to $1–T/T_c$, and a_i, with i varying from 1 to 6, are regressed coefficients that are determined from the fit of existing data, from the triple point of mercury to the critical point [17]. In such a model, the contribution to the pressure uncertainty arising from the propagation of the temperature uncertainty (0.01 K) turns out to be negligible.

Figure 3 reports the integrated absorbance data versus the atomic number densities for ^{200}Hg, resulting from the analysis of 210 spectra. The uncertainty on A_T is given by the standard deviation of repeated determinations. The densities (along with the corresponding uncertainties) are determined assuming a natural abundance for the mercury isotope in the vapor phase and using the ideal gas law [17]. More particularly, the abundances were 0.2310 (19) and 0.2986 (26), respectively, for ^{200}Hg and ^{202}Hg, as reported in Ref. [18]. A weighted linear fit was performed by taking into account the uncertainties on both the variables, A_T and N. As a result, the slope of the best-fit line is provided with a relative statistical uncertainty of about 0.3%.

As expected, the intercept turns out to be consistent with zero, a circumstance that shows the reliability of the entire procedure. Using Eqs. (3) and (4), a lifetime of 125.20 ±

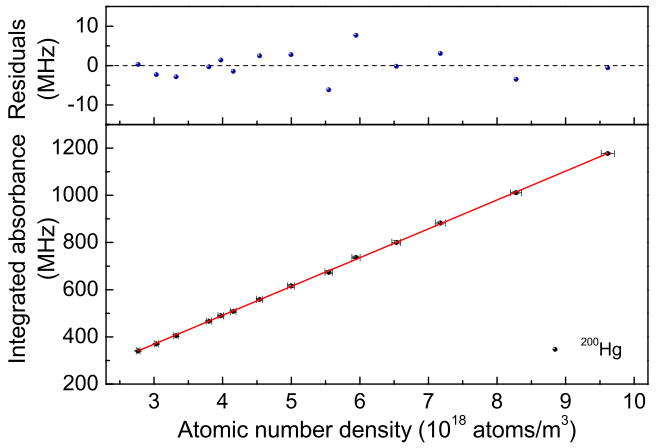

FIG. 3. Plot of the integrated absorbance data versus the atomic densities for the ^{200}Hg isotope. The weighted linear fit (red line) is shown along with the residuals (upper plot). We find a very good agreement between the data points and the best-fit line, with a linear correlation coefficient of 0.9998.

0.84 ns is retrieved. The uncertainty is the combined value of the statistical uncertainty (type A) resulting from the linear fit and the systematic deviations (type B) that are quoted in the uncertainty budget reported in Table I. It is useful to remember that, according to the Guide to the Expression of Uncertainty in Measurement [19], evaluations of uncertainty can be of the type A and type B. The former refers to a method of evaluation by statistical analysis of series of observations; the latter results from any means other than statistical analysis. The same procedure was followed for the ^{202}Hg isotope, leading to a lifetime of 125.03 ± 0.84 ns. The two measurements are consistent within 1σ, thus confirming the constancy of the lifetime across the individual mercury isotopes [20]. For the determination of the two lifetimes, we used the recent value of the line-center frequencies reported by Witkowski *et al.* [21]. The mean of the two values, considering 100%-correlated type B uncertainties, gives 125.12 ± 0.79 ns, with the statistical uncertainty being reduced down to 0.28 ns.

The main contribution to the uncertainty is given by the absorption path length. The cell length was measured by using a stainless steel electronic digital caliper, with a 0.01-mm resolution, before the optical bonding of the two windows. Taking into account the geometrical aperture of the vacuum chamber, it is possible to quantify the maximum deviation of the absorption path length from the cell length, due to a slight deviation of the UV beam from the normal incidence condition upon the cell. This upper limit turns out to be ≈ 2 μm. Therefore, a reasonable value for the deviation is 1 ± 1 μm. Such a contribution to the uncertainty budget is already included in the entry of Table I that is associated with the absorption path length.

TABLE I. Uncertainty budget related to the $^3P_1$ state lifetime.

Source	Type A (ns)	Type B (ns)
Statistical	0.40	
Absorption path length		0.70
FSR splitting frequency		0.25
Detector nonlinearity		Negligible
Optical zero		Negligible
Nonlinear effects		Negligible
Overall combined uncertainty	0.84	

The FSR frequency provides a second important contribution to the budget, as carefully quoted after repeating the spectral analysis with FSR values at the two extremes of the measured interval—namely, 299.72 MHz and 300.42 MHz. Using these two values, the retrieved lifetimes differ by 0.25 ns. Saturated absorption effects were estimated to be negligible, as the intensity of the probe UV beam is roughly three orders of magnitude smaller than the saturation intensity of the Hg line. A well-known source of error in the vertical scale is due to the possible occurrence of laser extra modes far from the atomic transition, causing an optical zero signal larger than the zero electric signal of the detector [22]. Using a much longer mercury cell to quantify the optical zero, we have experimentally verified that this effect is negligible, in our experimental conditions. Regarding SiC detector nonlinearity, we quoted the uncertainty on the lifetime determination due to a possible distortion of the observed profile by applying the procedure reported in Ref. [23], which is based upon numerical simulations of distorted profiles followed by line fitting. It turned out that any distortion caused by a detector nonlinearity did not add any measurable systematics.

To validate the experimental strategy and check the correctness of our assumptions, we determined the ^{200}Hg/^{202}Hg isotope ratio as a function of the gas temperature. No temperature-dependent fractionation effect was found at the present precision level. The weighted mean of the measured ratios amounts to 0.780 ± 0.001, with the uncertainty being 1–σ standard error of the mean. For comparison, the ^{200}Hg/^{202}Hg isotope ratio that results from the abundances reported in the National Institute of Standards and Technology database is equal to 0.774 ± 0.012 [18].

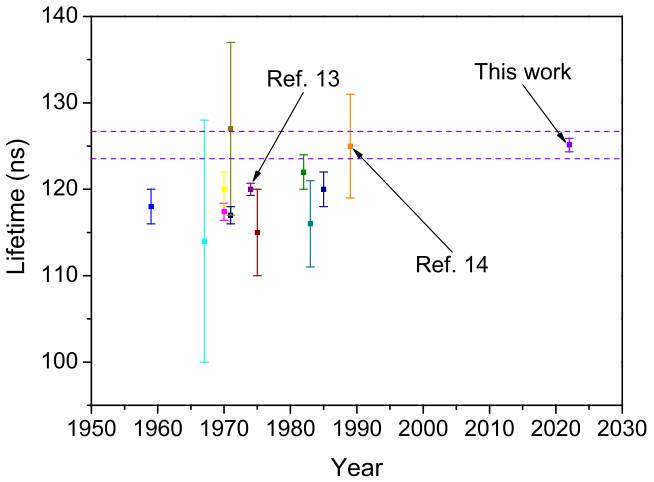

FIG. 4. Comparison with the 12 past determinations that are considered by Curtis *et al.* [12]. Error bars correspond to 1 standard deviation. The dashed lines identify the interval given by the measured value $\pm$ two times the quoted uncertainty of this work.

V. CONCLUSION

In conclusion, we measured the lifetime of the mercury $(6s6p)\ ^3P_1$ state for the isotopes with mass 200 and 202 using a novel approach based on linear absorption spectrometry in coincidence with the closed intercombination transition at 253.7 nm. A frequency chain from the near-infrared up to the deep UV allowed us to calibrate the spectra by means of the joint use of an optical resonator and a frequency comb synthesizer. We achieved a subpercent relative uncertainty, limited primarily by the uncertainty in the absorption path length. The comparison with the 12 prior determinations that are considered in Ref. [12] is shown in Fig. 4. Our value fully agrees with the latest determination from time-resolved laser-induced fluorescence spectroscopy [14], while being a factor of ∼8 more accurate. Instead, a slight mismatch is found with the best determination reported so far, given in Ref. [13]. The quantitative comparison shows an agreement with 8 of the 12 prior values within two times the stated uncertainties. Despite this, our value does not agree with the weighted average reported in Ref. [12].

This suggests that the average value reported by Curtis *et al.* [12] probably needs to be recalculated after a critical reassessment of the stated uncertainties, especially for the oldest determinations appearing in the database of past values.

ACKNOWLEDGMENTS

This research was funded by the Italian Ministry for University and Research (Program Type PRIN 2015) and by Università degli studi della Campania "Luigi Vanvitelli" within the V:ALERE program (Call published in 2019, Project V:ANS). The authors are grateful to Giuseppina Lopardo and Fabio Bertiglia for providing temperature traceability of the isothermal cell.

[1] P. Villwock, S. Siol, and Th. Walthera, Magneto-optical trapping of neutral mercury, Eur. Phys. J. D **65**, 251 (2011).

[2] M. D. Swallows, T. H. Loftus, W. C. Griffith, B. R. Heckel, E. N. Fortson, and M. V. Romalis, Techniques used to search for a permanent electric dipole moment of the ^{199}Hg atom and the implications for CP violation, Phys. Rev. A **87**, 012102 (2013).

[3] J. J. McFerran, L. Yi, S. Mejri, S. Di Manno, W. Zhang, J. Guéna, Y. Le Coq, and S. Bize, Neutral Atom Frequency Reference in the Deep Ultraviolet with Fractional uncertainty $= 5.7 \times 10^{-15}$, Phys. Rev. Lett. **108**, 183004 (2012).

[4] E. J. Angstmann, V. A. Dzuba, and V. V. Flambaum, Relativistic effects in two valence-electron atoms and ions and the search for variation of the fine-structure constant, Phys. Rev. A **70**, 014102 (2004).

[5] R. Wood, The selective reflection of monochromatic light by mercury vapor, Phil. Mag. **18**, 187 (1909).

[6] J. Lukusa Mudiayi, I. Maurin, T. Mashimo, J. C. de Aquino Carvalho, D. Bloch, S. K. Tokunaga, B. Darquié, and A. Laliotis, Linear Probing of Molecules at Micrometric Distances from a Surface with Sub-Doppler Frequency Resolution, Phys. Rev. Lett. **127**, 043201 (2021).

[7] C. R. Proffitt, T. Brage, D. S. Leckrone, G. M. Wahlgren, J. C. Brandt, C. J. Sansonetti, J. Reader, and S. G. Johansson, Mercury in the HgMn stars χ Lupi and HR 7775, Astrophys. J. **512**, 942 (1999).

[8] L. Dolk, G. M. Wahlgren, and S. Hubrig, On the elemental abundance and isotopic mixture of mercury in HgMn stars, Astron. Astrophys. **402**, 299 (2003).

[9] S. Ghazaryan and G. Alecian, Statistical analysis from recent abundance determinations in HgMn stars, Mon. Not. R. Astron. Soc. **460**, 1912 (2016).

[10] A. Srivastava and J. T. Hodges, Development of a high-resolution laser absorption spectroscopy method with application to the determination of absolute concentration of gaseous elemental mercury in air, Anal. Chem. **90**, 6781 (2018).

[11] A. Srivastava, S. E. Long, J. E. Norris, C. E. Bryan, J. Carney, and J. T. Hodges, Comparison of primary laser spectroscopy and mass spectrometry methods for measuring mass concentration of gaseous elemental mercury, Anal. Chem. **93**, 1050 (2021).

[12] L. J. Curtis, R. E. Irving, M. Henderson, R. Matulioniene, C. Froese Fischer, and E. H. Pinnington, Measurements and predictions of the $6s6p^{1,3}P_1$ lifetimes in the Hg isoelectronic sequence, Phys. Rev. A **63**, 042502 (2001).

[13] G. C. King and A. Adams, An accurate determination of the lifetime of the 6^3P state in mercury using a new electron-photon delayed coincidence apparatus, J. Phys. B Atom. Mol. Phys. **7**, 1712 (1974).

[14] E. C. Benck, J. E. Lawler, and J. T. Dakin, Lifetimes, branching ratios, and absolute transition probabilities in Hg i, J. Opt. Soc. Am. B **6**, 11 (1989).

[15] C. Clivati, S. Gravina, A. Castrillo, G. A. Costanzo, F. Levi, and L. Gianfrani, Tunable UV spectrometer for Doppler broadening thermometry of mercury, Opt. Lett. **45**, 3693 (2020).

[16] T. W. Hänsch and B. Couillaud, Laser frequency stabilization by polarization spectroscopy of a reflecting reference cavity, Opt. Comm. **35**, 441 (1980).

[17] M. L. Huber, A. Laesecke, and D. G. Friend, Correlation for the vapor pressure of mercury, Ind. Eng. Chem. Res. **45**, 7351 (2006).

[18] NIST Physical Measurement Laboratory. Database on atomic weights and isotopic compositions with relative atomic masses. https://www.nist.gov/pml/atomic-weights-and-isotopic-compositions-relative-atomic-masses.

[19] International Organization for Standardization. *Guide to the Expression of Uncertainty in Measurement* (International Organization for Standardization, Geneva, 1993).

[20] J. A. Halstead and R. Reeves, Determination of the lifetime of the mercury 6^3P_1 state, J. Quant. Spectrosc. Radiat. Transfer **28**, 289 (1982).

[21] M. Witkowski, G. Kowzan, R. Munoz-Rodriguez, R. Ciuryło, P. S. Żuchowski, P. Masłowski, and M. Zawada, Absolute frequency and isotope shift measurements of mercury $^1S_0 - {}^3P_1$ transition, Opt. Express **27**, 11069 (2019).

[22] A. Castrillo, G. Gagliardi, G. Casa, and L. Gianfrani, Combined interferometric and absorption-spectroscopic technique for determining molecular line strengths: Applications to CO_2, Phys. Rev. A **67**, 062503 (2003).

[23] H. Dinesan, S. Gravina, C. Clivati, A. Castrillo, F. Levi, and L. Gianfrani, Linearity of a silicon carbide photodiode in the deep-UV spectral region: Implications on Doppler broadening thermometry, Metrologia **57**, 065001 (2020).